Journal of
Applied Remote Sensing

RemoteSensing.SPIEDigitalLibrary.org

Optical characterization of two cyanobacteria genera, *Aphanizomenon* and *Microcystis*, with hyperspectral microscopy

Emily C. Paine
E. Terrence Slonecker
Nancy S. Simon
Barry H. Rosen
Ronald G. Resmini
David W. Allen

SPIE.

Emily C. Paine, E. Terrence Slonecker, Nancy S. Simon, Barry H. Rosen, Ronald G. Resmini, David W. Allen, "Optical characterization of two cyanobacteria genera, *Aphanizomenon* and *Microcystis*, with hyperspectral microscopy," *J. Appl. Remote Sens.* **12**(3), 036013 (2018), doi: 10.1117/1.JRS.12.036013.

Optical characterization of two cyanobacteria genera, *Aphanizomenon* and *Microcystis*, with hyperspectral microscopy

Emily C. Paine,[a] E. Terrence Slonecker,[a,*] Nancy S. Simon,[a] Barry H. Rosen,[a] Ronald G. Resmini,[b] and David W. Allen[c]

[a]U.S. Geological Survey, Reston, Virginia, United States
[b]MITRE Corporation, McLean, Northern Virginia, United States
[c]National Institute of Standards and Technology, Gaithersburg, Maryland, United States

Abstract. Cyanobacterial blooms are a nuisance and a potential hazard in freshwater systems worldwide. Remote sensing has been used to detect cyanobacterial blooms, but few studies have distinguished among genera of cyanobacteria. Because some genera are more likely to be toxic than others, this is a useful distinction. Hyperspectral imaging reflectance microscopy was used to examine cyanobacteria from Upper Klamath Lake, Oregon, at high spatial and spectral resolution to determine if two species found commonly in the lake, *Aphanizomenon flos-aquae* and *Microcystis aeruginosa*, can be separated spectrally. Of the analytical methods applied, a spectral shape algorithm applied to the derivative was found to be most successful in classifying these species in microscope scenes. Further work is required to determine if the spectral characterization of cyanobacterial genera can be scaled up to remote sensing applications. [DOI: 10.1117/1.JRS.12.036013]

Keywords: harmful algal blooms; hyperspectral microscopy; cyanobacteria; microcystis; imaging spectroscopy; derivative analysis.

Paper 170730 received Aug. 17, 2017; accepted for publication Aug. 14, 2018; published online Sep. 4, 2018.

1 Introduction

Cyanobacterial blooms in eutrophic inland waters are a worldwide concern. Blooms are exacerbated by high nutrient inputs and warm waters and have been appearing with increasing frequency in water bodies used for drinking water supply or recreation, a problem which will likely worsen as the climate warms.[1–3] Cyanobacterial blooms are a nuisance for their unsightly surface scums and the production of taste-and-odor compounds, and some strains of cyanobacteria produce toxins that are hazardous to human and animal health.[4] Toxic cyanobacterial harmful algal blooms, or cyanoHABs, are not immediately distinguishable from nontoxic nuisance blooms; laboratory analysis is required to identify the species present and test for toxins.[2] For large water bodies, collecting point samples is insufficient to quantify the true extent of the toxic algae, particularly as blooms are often heterogeneous and dynamic.[5]

Some of the most widespread cyanobacterial toxins are microcystins. Microcystins are potent hepatotoxins that can cause illness and death in exposed animals and humans, and over 100 variants are known Ref. 6. Microcystins are released by several genera of cyanobacteria, including *Microcystis*, *Planktothrix*, and *Dolichospermum*, but toxin production is not guaranteed by the presence of these organisms. Blooms of *Microcystis*, for example, may consist of strains of microcystin-producing and nonmicrocystin-producing cells distinguishable only by laboratory analysis of gene expression.[2] Higher nutrient concentrations and increased temperature may favor the growth of microcystin-producing strains.[2] With toxic blooms potentially growing

*Address all correspondence to: E. Terrence Slonecker, E-mail: tslonecker@usgs.gov

more dangerous, the ability to determine the extent of toxic genera within a bloom would be valuable.

For many years, remote sensing has been used to map algal blooms. Mapping of chlorophyll *a* is widely used as an indicator of water quality, but because both eukaryotic algae and cyanobacteria contain chlorophyll, chlorophyll a can suffer from a lack of specificity and is most successful in blooms that are known to be dominated by cyanobacteria.[7] An alternative is using the accessory pigment phycocyanin, produced by cyanobacteria but not by many other phytoplankton, as a proxy.[1,8–10] However, methods that measure phycocyanin in the laboratory are not standardized, and phycocyanin is less easily detected with remote sensing.[7] Another approach is the cyanobacteria index, which uses the absorption feature at 681 nm to distinguish cyanobacteria from eukaryotic algae.[7] Chlorophyll *a* in eukaryotic algae fluoresces at 681 nm, but chlorophyll *a* in cyanobacteria is contained in photosystem I and does not fluoresce, so the signal at this wavelength is dominated by chlorophyll absorption and the difference in spectral shape can be quantified to determine the type of algae present.[7]

Recently, there has been an increase in the availability of hyperspectral imaging sensors that can measure over 30 narrow bands (usually over 100 bands) to produce a complete, high-resolution spectrum. These spectra may reveal details that were previously invisible to sensors with fewer bands, opening a path to the development of new models that consider the entire spectrum. Kudela et al.[11] made use of a spectral shape algorithm to discriminate *Aphanizomenon*, a nontoxic genus in many water bodies, from *Microcystis* in California lakes. The *Aphanizomenon-Microcystis* index uses a ratio of the width of the major chlorophyll *a* reflectance feature to the width of the phycocyanin absorption feature and was developed using aerial hyperspectral imagery. The algorithm provides an estimate of the relative abundance of *Microcystis* and *Aphanizomenon* in a pixel and was calibrated with measured cell counts.[11]

The high-resolution spectra provided by hyperspectral imaging sensors also invite other analysis techniques, such as the spectral derivative. Hunter et al.[12] used first-derivative analysis to discriminate among phytoplankton color groups, although the study was not particularly focused on separating cyanobacterial genera. The spectral derivative accentuates differences among spectra that might not otherwise be apparent, providing a useful tool for the separation of spectrally similar species.

The spectral similarity of some cyanobacterial genera is a major obstacle to identifying blooms of potentially toxic genera. However, in this case, the ability to spectrally distinguish among the genera is desirable for several reasons. First, not all cyanobacteria produce toxins in all environments, so locating areas that are more at-risk for toxin production is a priority. This knowledge could help water managers decide where to collect water samples for toxin analysis. In addition, the ability to identify different genera could lead to an improved understanding of bloom dynamics, particularly in cases with spatially or temporally heterogeneous blooms. This study aimed to undertake a close examination of *Aphanizomenon flos-aquae* and *Microcystis aeruginosa* to determine if these two common species are spectrally separable. To this end, a hyperspectral microscope at the National Institute of Standards and Technology (NIST) was employed to study algal samples from Upper Klamath Lake (UKL) in Oregon. The hyperspectral microscope allows for the study of cyanobacteria at high spatial and spectral resolution and in a controlled environment, without the interference of variable sunlight or cloud conditions. In this way, cyanobacteria and other associated organisms can be characterized at the organismal level. In future work, this characterization could ideally be used for target identification of cyanobacterial genera in remote sensing data collected with hyperspectral sensors.

2 Study Site and Methods

2.1 *Study Site*

UKL in Oregon, and (Fig. 1) consistently experiences cyanobacterial blooms each summer. The shallow lake (3-m average depth) has become increasingly eutrophic due to human activity, such as the draining of wetlands for agriculture, which has resulted in higher nutrient inputs.[13] Cyanobacteria blooms are so persistent and extensive that an industry has developed around

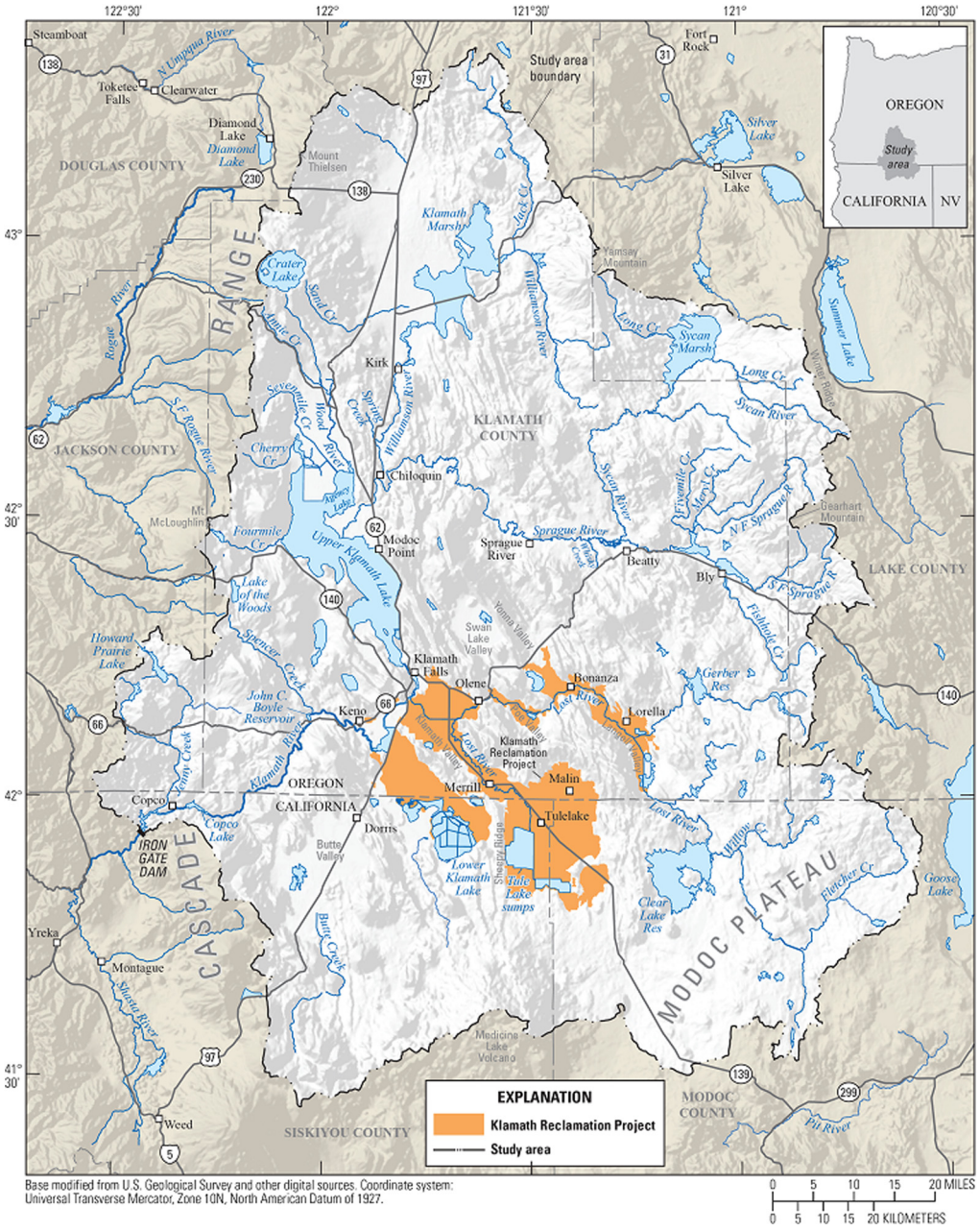

Fig. 1 Location of UKL, Oregon.

one of the lake's most common genera, *A. flos-aquae*, which is harvested from the lake and sold as a health supplement. Although some strains of *Aphanizomenon* have been shown to produce toxins, the *A. flos-aquae* has not been found to be toxic in UKL.[14] However, *Microcystis* is also consistently present in the lake and does produce microcystins in this environment, which is a problem for both the harvesting of *Aphanizomenon* as well as the recreational activities on the lake. Blooms in this region often proceed from a progression of dominance by *Aphanizomenon*, followed by mixed blooms, and then by dominance of *Microcystis*, sometimes with multiple cycles in one season and typically in mid- to late-summer.[11] The prolonged appearance of these blooms is also thought to affect the fish populations in the lake, particularly two species of endangered suckers, because the oxygen demand of decaying blooms can lead to hypoxic conditions.[13]

The same four general locations on UKL were sampled in summer 2016, from July 15, 2016 (week 1) to September 15, 2016 (week 10). Raw water samples were collected in opaque plastic bottles, chilled and sent overnight to NIST for spectral analysis. Samples were processed as soon

as they were received or refrigerated until they could be processed. Wet slides were prepared with algae taken from the top of each sample bottle. A reference slide was prepared with distilled water and cover glass.

2.2 *Hyperspectral Microscope*

The NIST hyperspectral microscope consists of two parts: the microscope component is an Olympus MVX-10 microscope with an MX-2X Objective and a 1 to 4× magnification changer, and the hyperspectral imaging component is a Surface Optics SOC-710 hyperspectral camera (Surface Optics, San Diego, California). The SOC-710 measures 128 spectral bands, at 4.69 nm spectral sampling over the 400 to 1000 nm spectral range. The finest spatial resolution of the system is on the order of <0.2 μm/pixel. Illumination was provided by three quartz-halogen lamps set with dichroic reflectors to match the solar spectrum with a high color temperature.

Before sample measurement, reference data cubes were collected from the reference slide placed on top of a Spectralon® disk (Labsphere, North Sutton, New Hampshire), and integration times were optimized for each desired magnification level. Data cubes were then collected from the sample slides, generally one slide per sample bottle. Depending on integration time, image acquisition took between 2 and 15 min to complete. Two to 10 images were collected per slide, depending on algal abundance. A fresh reference slide was measured after data collection was finished, 4 to 6 h later. Slides were kept out of direct light when not being measured. Figure 2 shows examples of the true color composites from the hyperspectral microscope images.

2.3 *Data Analysis*

Data cubes were normalized in ENVI (Exelis, Boulder, Colorado) to the reference data cube. A principal component (PC) transformation was applied to a spectral subset of bands 7 to 65 (402.5 to 701.1 nm) to avoid the noisy regions of the spectrum. The spectral derivative of each cube was calculated with the ENVI user function "Spectral_Derivative." The derivative transformation was applied to a subset of bands 13 to 59 (432.6 to 669.5 nm) to encompass the main features that were observed to differ between the derivative spectra of *Microcystis* and *Aphanizomenon.* Basic statistical and hyperspectral processing techniques were utilized to determine the separability of the spectral classes in this and many other applications. Both principal components analysis (PCA) and derivative transformations help determine the separability of basic algal signatures.

The normalized data, the PC data, and the derivative data were then analyzed with several of the algorithms and classification methods included in ENVI to evaluate the separability of *Microcystis* and *Aphanizomenon.* PCA was used to determine quickly whether different genera

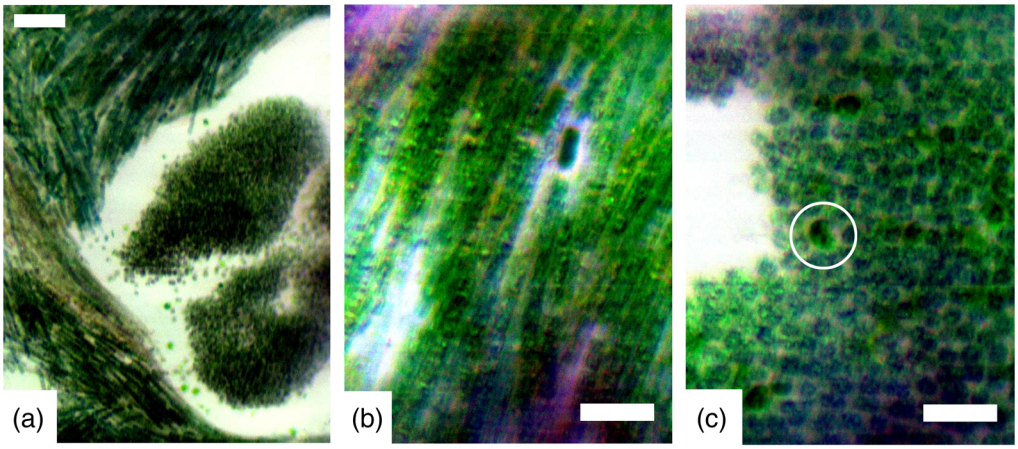

Fig. 2 True color composites derived from data cubes collected by the hyperspectral microscope. (a) *Aphanizomenon*, *Microcystis*, and green algae. (b) *Aphanizomenon* at full magnification, with a visible heterocyte. (c) *Microcystis* at full magnification, with green algae (circled). Scale bars are 50, 20, and 20 μm, respectively.

were dissimilar enough to classify separately. These transformed datasets were chosen as basic hyperspectral processing techniques that are used to determine if specific spectral signatures are separable in a dataset.

Analysis of the normalized and derivative spectra was carried out using the ENVI linear spectral unmixing algorithm. Endmembers were collected from the input image as representative cells and example images from the week of August 8 (week 5) were chosen to extract representative spectra for *Aphanizomenon*, *Microcystis*, and green algae because they represented outstanding visual examples of the target species and spectra. These endmembers were used to apply the unmixing algorithm to all 6 weeks of imagery. See the Appendix for additional spreadsheets and graphics of data transformations.

Additional analysis took the form of multiband algorithms sensitive to spectral shape. The spectral shape equation [Eq. (1)] was adapted to be applied to the first derivative spectra to separate *Aphanizomenon* and *Microcystis*.[7] The adapted equation is shown in Eq. (2) and is referred to as the derivative spectral shape (derivSS) equation. This was applied to two sections of the spectra, at 468 and 509 nm, where the shape of the derivative was observed to differ significantly from *Aphanizomenon* to *Microcystis* (Fig. 3 and Index 1)

$$\mathrm{SS}(\lambda) = R(\lambda) - R(\lambda^-) + \{R(\lambda^-) - R(\lambda^+)\} \times \frac{(\lambda - \lambda^-)}{(\lambda^+ - \lambda^-)}, \tag{1}$$

$$\mathrm{derivSS}(\lambda) = \frac{dR}{d\lambda}(\lambda) - \frac{dR}{d\lambda}(\lambda^-) + \left\{\frac{dR}{d\lambda}(\lambda^-) - \frac{dR}{d\lambda}(\lambda^+)\right\} \times \frac{(\lambda - \lambda^-)}{(\lambda^+ - \lambda^-)}, \tag{2}$$

where SS is the spectral shape, λ is the wavelength, and R is the value of the calibrated reflectance. For derivSS(468), $\lambda^- = 452$ nm and $\lambda^+ = 478$ nm. For derivSS(509), $\lambda^- = 488$ nm and $\lambda^+ = 529$ nm (Index 2). The wavelengths were chosen to encompass the peak features observed in the *Microcystis* derivative spectrum at these locations, based on manual observations of spectra drawn from several. Dataset weeks of samples.

A third index was also employed, the slope of the derivative curve from 628 to 632 nm. This index was chosen because 628 nm was the location of the phycocyanin absorption feature for *Aphanizomenon*, so the index was positive, while for *Microcystis*, the phycocyanin feature occurred at a shorter wavelength and the index was less positive (data not shown). In addition, the slope of the derivative for green algae at this point is negative. These three indices served to demonstrate that the spectral features that appeared to differ between the two genera in region-of-interest (ROI) average spectra were consistent across all the imagery collected.

For some instances, a dataset was prepared consisting of single-cell ROIs from nearly all images collected in the final 6 weeks. Between three and six ROIs were designated in each

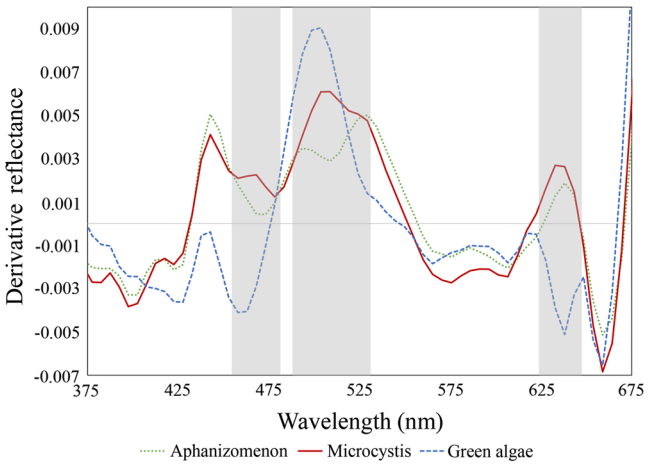

Fig. 3 Derivative spectra of *Aphanizomenon* and *Microcystis*, with differing features at 468, 509, and 628 nm circled. This plot shows a subset of the full wavelength range of the hyperspectral microscope.

image, resulting in a dataset with 165 samples of *Aphanizomenon* and 195 samples of *Microcystis.* In addition, ROIs for other organisms found in the samples, such as diatoms, green algae, and other cyanobacteria, were catalogued and included in this dataset. Average values from these ROIs were used to assess the ability of different algorithms to separate genera. The "ROI dataset" in the following discussion refers to this collection of spectra. For each week, a mosaic image was constructed with all the data collected at the highest magnification so classification methods could be tested on images with more spectral variation.

3 Results

3.1 *Observations*

Hyperspectral image cubes collected during the final 6 weeks of sampling, August 8th to September 15th, were used in analysis because a different data collection method was used for the first 4 weeks and the cubes are not comparable.

Gas vesicles are visible in both *Microcystis* and *Aphanizomenon* cells. Heterocytes (nitrogen-fixing cells) and akinetes (resting cells) were observed in *Aphanizomenon* filaments. Both *Microcystis* and *Aphanizomenon* were observed in week 1 (July 13, 2016) through week 7 (August 22), but week 8 (August 29) was dominated by *Microcystis*, and *Aphanizomenon* was less plentiful in weeks 9 and 10. This reduction corresponded well with recorded cell counts from these weeks (data not shown).

Various unspecified green algae were observed throughout *Microcystis* colonies, beginning the week of August 8 (week 5). An unidentified cyanobacterium was associated with *Microcystis* colonies in week 6. Protozoans were observed grazing on *Microcystis* during weeks 9 and 10, as the bloom died off. Pennate diatoms were also observed during these weeks. These observations potentially underestimate the diversity of the phytoplankton population because only a small fraction of the algae in the sample bottle was transferred to a slide.

In general, the reflectance spectrum for cyanobacteria consists of a Chl-*a* reflectance peak at 565 nm, phycocyanin absorption at 620 nm, and Chl-*a* absorption at 680. Both *Aphanizomenon* and *Microcystis* spectra include these features, and the spectra of green algae lack the phycocyanin feature. Figure 4 shows sample spectra from the major taxa present in the UKL samples.

Although the major spectral features were similar for all algae, there was significant variation with each genus. *Aphanizomenon* and *Microcystis* were both observed in a range of colors from yellow-green to blue-green.

It should also be noted that spectral areas of traditional vegetation analysis, the red edge and the near-infrared (NIR) slope, did not lend themselves to spectral distinction between the algal species. This was likely due to the mixed-media environment of partially submerged vegetation

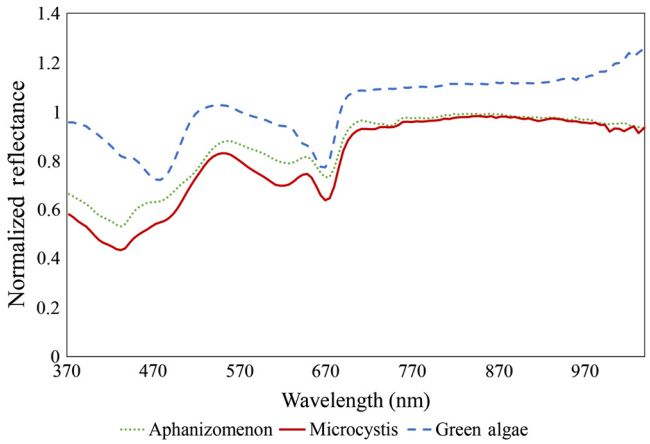

Fig. 4 Example spectra from cells of *Aphanizomenon* (green), *Microcystis* (red), and green algae (blue). Reflectance at 565 nm and absorbance at 680 nm is indicative of chlorophyll *a*, while absorbance at 620 nm is indicative of phycocyanin.

in water, and this could prove to be an important departure from standard hyperspectral vegetation analysis.

3.2 *Data Analysis*

The linear spectral unmixing algorithm returned the most accurate results compared to other ENVI classification methods (Fig. 5), but still resulted in misclassified pixels. Figure 6(a) shows the average abundance values returned by the algorithm over single cell ROIs. Points above the 1:1 line are classified as *Aphanizomenon* and points below are classified as *Microcystis*. Misclassified pixels could be dangerous from a false positive/false negative standpoint. Unclassified pixels are not useful, but in the hyperspectral microscope imagery, there were generally enough classified pixels in an area to infer the identity of the unclassified ones. This should be less of a problem with imagery of increasing areal extent, capturing more pixels.

Data transformations such as the spectral derivative accentuated the subtle, consistent differences between *Aphanizomenon* and *Microcystis* spectra. Figure 5(b) shows how the

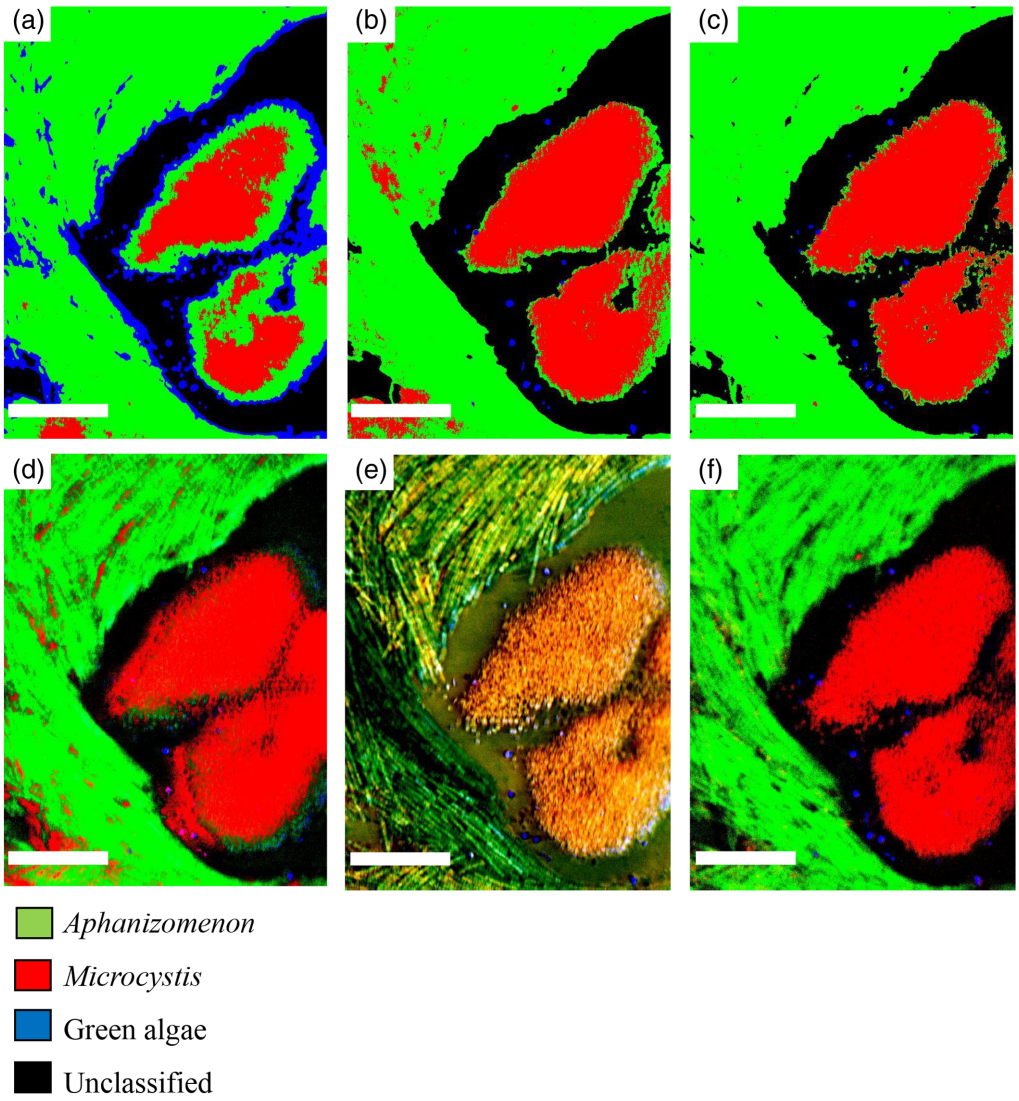

Fig. 5 (a, d) Classification methods applied to normalized images, (b, e) PC transformations, and (c, f) spectral derivative transformations of the scene shown in Fig. 2(a). Both (a–c) the support vector machine classification and (d–e) the linear spectral unmixing algorithm were most successful when applied to derivative transformations. The unmixing maps have been optimized with contrast stretching. Scale bars are 100 μm.

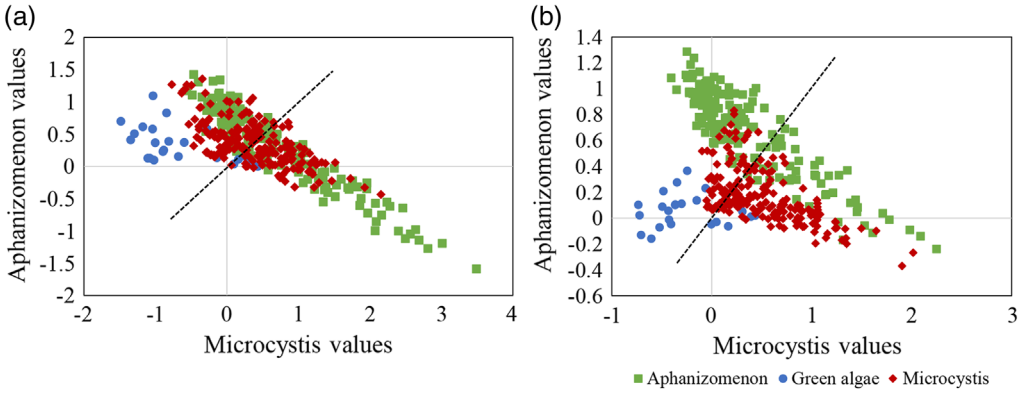

Fig. 6 (a) Average linear spectral unmixing values for the ROI dataset. (b) Average linear spectral unmixing values for the ROI dataset after derivative transformation. Points above the 1:1 line are classified as *Aphanizomenon* and points below are classified as *Microcystis*. Red diamonds are cells identified in the imagery as *Microcystis*; green squares, *Aphanizomenon*; and blue circles, green algae.

two cyanobacterial genera became more separable after the derivative transformation. However, the mapping algorithms still resulted in errors, and differentiated cells and color variations still led to some incorrectly classified pixels. For the ROI dataset, 70% of *Aphanizomenon* and 69% of *Microcystis* were classified correctly.

However, keep in mind that there are other cellular variations and structures within the matrix of features in the typical algal sample, not just the pure algal species. These components and variations have different structural components and different color variations and lead to some incorrectly classified pixels, especially when mapping algal species. Classification applied to PC transformations was less successful than the same process applied to derivative data, resulting in more misclassified pixels [Fig. 5(e)].

The derivative spectral shape indices were developed to determine if classification could be improved by focusing on key segments of the spectrum, and to determine if the unique spectral features observed for each genus were applicable across all the imagery collected. The indices focus only on the wavelengths at which *Aphanizomenon* and *Microcystis* differ the most, taking advantage of peaks and troughs that are accentuated by the derivative transformation. The derivSS(468) and derivSS(509) were observed to be more positive for *Microcystis*, while the second derivative at 628 nm is close to zero for *Microcystis* and positive for *Aphanizomenon*. In addition, the second derivative at 628 nm is markedly negative for green algae. The values of the derivative indices applied to the ROI dataset are shown in the scatterplot in Fig. 7. This scatterplot was used to develop thresholds for each class, which were applied to data cubes

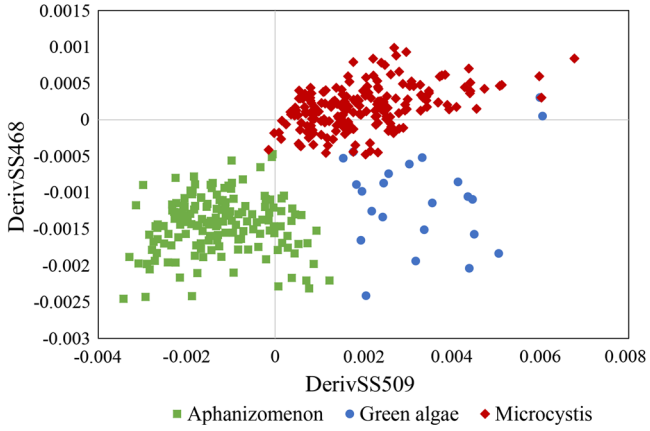

Fig. 7 Derivative spectral shape values of the ROI dataset. Class thresholds were established based on this plot and on a plot of the second derivative at 628 nm.

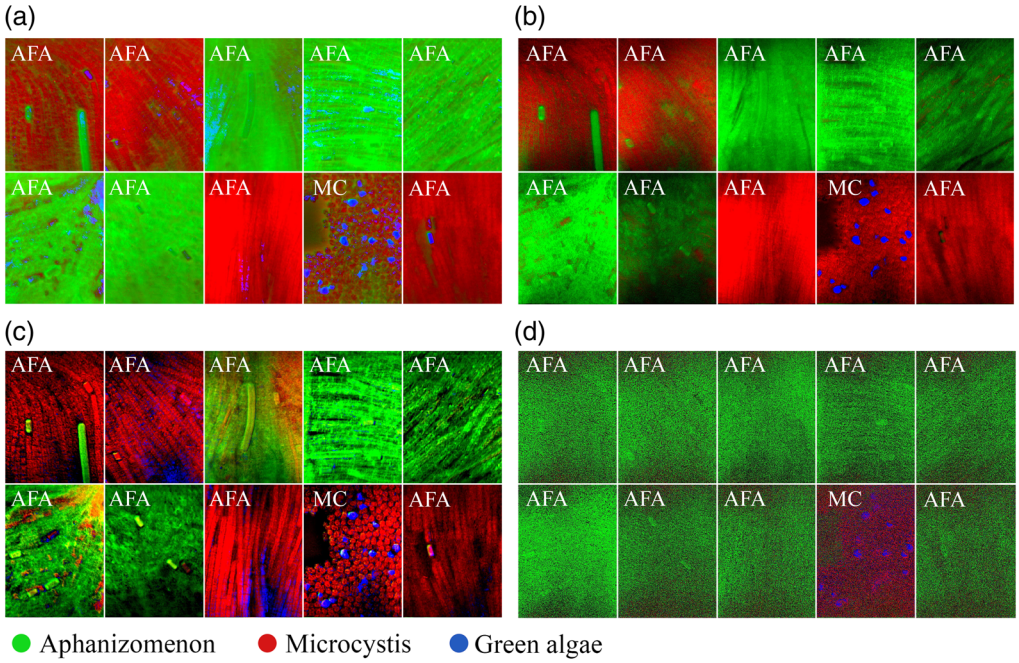

Fig. 8 Mosaics of week 5 imagery after different classification methods. Each image is labeled with the manually identified genus, AFA for *Aphanizomenon* and MC for *Microcystis*. (a) Linear spectral unmixing of normalized data. (b) Linear spectral unmixing of derivative data. (c) Linear spectral unmixing of PC data. (d) Derivative spectral shape index classification. Red pixels have been classified as *Microcystis*; green, *Aphanizomenon*; blue, green algae. All unmixing algorithms included the three genera and a background endmember. Contrast stretching was applied to optimize each unmixing map.

to construct classification images. Pixels for which all three indices match the criteria for a given class were assigned the designated color for that class, and pixels that failed a single criterion were left unclassified. Of all classification methods used, the method based on the spectral shape indices resulted in the fewest misclassified pixels. Figure 8 shows a mosaic of images from week 5, classified with linear spectral unmixing and with the derivative spectral shape indices. The derivative spectral shape indices resulted in fewer misclassifications than the linear spectral unmixing algorithm (Fig. 8). In the ROI dataset, 96% of *Microcystis* cells were classified correctly, and 100% of *Aphanizomenon* cells were classified correctly, in this case meaning that the number of pixels in the ROI classified as the observed cell genus was greater than the number of classified genus, disregarding unclassified pixels.

4 Discussion

The goal of this pilot study was to determine if *Aphanizomenon* and *Microcystis* have unique spectral features. With hyperspectral microscope imagery collected from UKL water samples over 6 weeks, it was determined that these features exist and can be accentuated through derivative transformation. In hyperspectral microscope scenes, *Aphanizomenon* and *Microcystis* can be treated as individual target materials and can be classified accordingly. The success of the derivative spectral shape equations shows that the spectral differences are consistent across all the imagery collected from UKL samples in summer 2016. It is not known from this study precisely what causes the differences in *Aphanizomenon* and *Microcystis* spectra.

The hyperspectral microscope operates under laboratory conditions, but further study is required to determine if those conditions affect the cells adversely. Slides were kept in the dark when not under the microscope, but because the pushbroom scan requires high integration times (~650 ms/line) at high magnifications, a single slide was often under the illumination source for an hour or more. This study did not examine the effects that these conditions may have had on the spectra, and that is an area for further research.

The derivative spectral shape indices will not be applicable to other datasets without adjustments. They are also unlikely to be useful in systems with different cyanobacteria populations. However, the spectral shape indices demonstrate that identifying key features for certain genera and classifying based on these features, instead of using the entire spectrum, could improve identification. A similar approach is taken by the U.S. Geological Survey program Tetracorder, which matches continuum-removed field spectra against a library of spectral features to identify minerals, using only features previously identified as characteristic of a mineral to generate the best match.[15] Continuum removal was explored only briefly in this study, but a similar process with derivative spectra could be developed for cyanobacteria.

As this is a pilot study, future work is required to determine the applicability of these results to remotely sensed data. It is acknowledged that observations made on the microscope scale may not be detectable in remote sensing data of natural waters. Natural waters, particularly in eutrophic inland systems, are complex and there is potential for these fine spectral features to be obscured. Microcosm or mesocosm experiments in the laboratory or in the field could be developed to determine the effect of colored dissolved organic matter and inorganic sediment on the spectral features. Hunter et al.[12] reported that suspended particulate organic matter added to phytoplankton mesocosms altered spectral shape, thus reducing the ability of derivative analysis to distinguish between taxa.

Analyses such as the derivative spectral shape equations were applied to the data to determine if the features observed were present throughout the imagery, but the success of those methods does not necessarily indicate that the spectral features are universal across each genus. Color variation observed in UKL samples led to a higher proportion of misclassified or unclassified pixels, and variations occurring over multiple seasons or in different lake systems will add further complications. A spectral library developed from lake samples and cultures would be a step toward overcoming this issue.

Pigment variability due to cell metabolism and environmental conditions is another obstacle to the optical characterization of different genera, because different conditions can have a significant effect on pigment composition and therefore spectral response.[5,12] This was evident in the UKL samples, both in the observed color variation under the microscope and in the range of spectra collected for each genus. However, this variation could also provide insight into water quality. If changes in the spectrum resulting from interactions of cell pigments with the environment can be constrained, then spectral analysis might provide further information in addition to species identification. A microfluidics chip could be used to establish a nutrient gradient on the scale of the hyperspectral microscope, which could then record the spectral response of cells to different concentrations.[16] In addition, further microscope analysis of dead and dying cell material is needed to determine if crashing blooms have a characteristic signature.

The ability to detect specific genera of cyanobacteria could lead to improved estimates for toxin concentrations. Algorithms developed to estimate toxin concentration generally use the spectral features associated with chlorophyll a or phycocyanin, and then use measurements and models to determine relationships that exist between toxin concentration and pigments.[12] However, these relationships assume that toxins are intracellular and uniformly distributed through a bloom, which is not necessarily the case, especially in heterogeneous blooms.[12] The ability to constrain toxin predictions to only the areas that contain toxic genera could improve the accuracy of such maps. However, this does not address the problem of extracellular toxins. Dissolved toxins such as microcystin have no spectral signature in the visible or NIR wavelengths.[7] Since toxins are released upon cell lysis, the presence of decaying blooms is a useful indicator of when high levels of toxin might be present. However, it should be noted that toxin levels may not correlate spatially with bloom biomass, and toxins may persist even after the bloom has dissipated.[5]

5 Conclusion

Aphanizomenon and *Microcystis* have unique spectral features that can be distinguished with hyperspectral microscopy. The spectral derivative is useful for accentuating these features.

Algorithms applied to the spectral derivative were more successful in classifying genera correctly, and identifying cyanobacteria by a few characteristic features instead of the entire spectrum yielded improved results. The results indicate that there is value in the spectral characterization of cyanobacteria. Further research is required to determine if these spectral features can be detected in smaller-scale, overhead, remote sensing data.

Acknowledgments

Funding for this work was provided by the U. S. Geological Survey Land Remote Sensing Program. Research was conducted at and with the cooperation of the National Institute of Standards and Technology (NIST) in Gaithersburg, Maryland, USA. We acknowledge Eric Tvinnereim for his work in the field at Upper Klamath Lake. A brief description of these results was published in Ref. 17. Data used in this project were reviewed and published in Sciencebase.[18] Notice: Any use of trade, firm, or product names is for descriptive purposes only and does not imply endorsement by the U.S. Government.

References

1. L. Li et al., "Using hyperspectral remote sensing to estimate chlorophyll-a and phycocyanin in a mesotrophic reservoir," *Int. J. Remote Sens.* **31**(15), 4147–4162 (2010).
2. J. M. O'Neil et al., "The rise of harmful cyanobacteria blooms: the potential roles of eutrophication and climate change," *Harmful Algae* **14**, 313–334 (2012).
3. H. W. Paerl et al., "Harmful freshwater algal blooms, with an emphasis on cyanobacteria," *Sci. World* **1**, 76–113 (2001).
4. W. W. Carmichael, "Heath effects of toxin-producing cyanobacteria: 'The CyanoHABs'," *Hum. Ecol. Risk Assess.* **7**(5), 1393–1407 (2001).
5. P. D. Hunter et al., "Hyperspectral remote sensing of cyanobacterial pigments as indicators for cell populations and toxins in eutrophic lakes," *Remote Sens. Environ.* **114**, 2705–2718 (2010).
6. T. Niedermeyer, "Microcystin congeners described in literature" (2013), http://dx.doi.org/10.6084/m9.figshare.880756.
7. R. P. Stumpf et al., "Challenges for mapping cyanotoxin patterns from remote sensing of cyanobacteria," *Harmful Algae* **54**, 160–173 (2016).
8. R. K. Vincent et al., "Phycocyanin detection from LANDSAT TM data for mapping cyanobacterial blooms in Lake Erie," *Remote Sens. Environ.* **89**, 381–392 (2004).
9. S. G. H. Simis, S. W. M. Peters, and H. J. Gons, "Remote sensing of the cyanobacterial pigment phycocyanin in turbid inland water," *Limnol. Oceanogr.* **50**(1), 237–245 (2005).
10. K. Randolph et al., "Hyperspectral remote sensing of cyanobacteria in turbid productive water using optically active pigments, chlorophyll a and phycocyanin," *Remote Sens. Environ.* **112**, 4009–4019 (2008).
11. R. M. Kudela et al., "Application of hyperspectral remote sensing to cyanobacterial blooms in inland waters," *Remote Sens. Environ.* **167**, 196–205 (2015).
12. P. D. Hunter et al., "Spectral discrimination of phytoplankton colour groups: the effect of suspended particulate matter and sensor spectral resolution," *Remote Sens. Environ.* **112**, 1527–1544 (2008).
13. D. T. Snyder and J. L. Morace, "Nitrogen and phosphorus loading from drained wetlands adjacent to Upper Klamath and Agency Lakes, Oregon," USGS Water-Resources Investigations Report 97–4059 (1997).
14. W. W. Carmichael et al., "Harvesting of Aphanizomenon flos-aquae Ralfs ex Born. & Flah. var. flos-aquae (Cyanobacteria) from Klamath Lake for human dietary use," *J. Appl. Phycol.* **12**, 585–595 (2000).
15. R. N. Clark et al., "Imaging spectroscopy: earth and planetary remote sensing with the USGS Tetracorder and expert systems," *J. Geophys. Res.* **108**(E12), 1–44 (2003).
16. J. Atencia, G. A. Cooksey, and L. E. Locascio, "A robust diffusion-based gradient generator for dynamic cell assays," *Lab Chip* **12**, 309–316 (2012).

17. E. T. Slonecker et al., "Full-range, solar-reflected hyperspectral microscopy to support earth remote sensing research," *J. Appl. Remote Sens.* **12**(2), 026024 (2018).
18. E. T. Slonecker, E. C. Paine, and N. S. Simon, "Hyperspectral image microscopy of harmful algal bloom samples from Upper Klamath Lake, Oregon, 2016," U. S. Geological Survey Data Release (2017), https://www.sciencebase.gov/catalog/item/5b61f93ae4b006a11f6f789b.

Emily C. Paine earned a bachelor's of science in earth science from Rice University. She recently went on to work with the U.S. Geological Survey on a project to identify the spectral characteristics of cyanobacteria using hyperspectral microscopy. She now works as a lab technician and is pursuing graduate opportunities.

E. Terrence Slonecker is a research geographer with the USGS. He specializes in remote sensing and other geospatial analyses of hazardous waste and other fugitive contaminants His current research interests include VIS/NIR/FTIR spectroscopy and imaging spectroscopy. He holds a master's degree in geography and a doctorate in environmental science, both from George Mason University. With 30+ years of experience with the U.S. Air Force, the U.S. environmental protection agency and the U.S. Geological Survey, he has served on many special assignments including the Gore-Chernomrydin Commission, the Civil Application Committee, the spring valley world war 1 chemical weapons cleanup and has recently served as a remote sensing instructor in Afghanistan.

Nancy S. Simon is a research chemist with the USGS and has been working to expand our understanding of the forms of nutrients (phosphorus) in lake and river sediments and develops models for the movement of nutrients between water, sediment and biota. Her studies focus on processes that lead to the release or retention of phosphorus (P) from sedimentary environments. Processes of interest to her projects include, but not limited to, P interactions with clays, organic matter, and poorly crystalline iron (Fe) oxides. Nancy's project examines the forms (species) of metals and nutrients in sedimentary environments, that is, oxidation-reduction conditions in sediments, the presence of complexing ligands, and mineral formation or dissolution. She holds a doctorate in chemistry from American University in Washington, DC.

Barry H. Rosen is a research biologist with the USGS and supervises a funded research program in algae, including work on the identification and genetics of cyanobacteria, cyanotoxin methods development, the potential linkage between cyanobacterial toxins and ALS, and diatom taxonomy. He specializes in the flora of various freshwater and marine waterbodies in the U.S., with emphasis on the Everglades. He is a senior research associate, with the University of Central Florida. He holds a PhD in biology from Bowling Green State University, Bowling Green, Ohio.

Ronald G. Resmini is a research scientist in the Advanced ISR Department of the MITRE Corporation and an adjunct associate professor in the College of Science at George Mason University, Fairfax, Virginia. He specializes in visible to infrared multi- and hyperspectral imagery remote sensing; the geological and geophysical sciences; the analysis, design, and development of algorithms for processing and analysis of remotely sensed information; and modeling of natural processes observed in remotely sensed data.

David W. Allen is a research chemist at the National Institute of Standards and Technology, (NIST), in Gaithersburg, Maryland. He holds a bachelor's degree in Chemistry and a master's in environmental biology, both from Hood College, and a PhD in earth systems and geoinformation science (remote sensing) from George Mason University. He currently works in the Sensor Sciences Division at NIST and leads research in the areas of medicine, environment, and defense using hyperspectral imaging for detection and quantitative analysis.